Ceramics-Silikáty 64 (2), 155-163 (2020)
www.ceramics-silikaty.cz doi: 10.13168/cs.2020.0004

THE SHRINKAGE, PHASE COMPOSITION AND MECHANICAL PROPERTIES OF CERAMICS WITH DIFFERENT β-SiAlON MAIN CRYSTALLINE PHASES PREPARED BY STEREOLITHOGRAPHY

#ZHUO TIAN*, YUPING YANG*, YONG WANG**, HAIDONG WU*, WEI LIU*, #SHANGHUA WU*

*School of Electromechanical Engineering, Guangdong University of Technology, Guangzhou 510006, Guangdong, China
**Dongguan South China Design Innovation Institute, Dongguan 523808, Guangdong, China

#E-mail: tianzhuo@gdut.edu.cn, swu@gdut.edu.cn

Submitted August 30, 2019; accepted November 20, 2019

Keywords: SiAlON, Additive manufacturing, Mechanical properties, Sintering

In this paper, using Si_3N_4, Al_2O_3 and AlN particles as raw materials, β-SiAlON ceramics with different main crystal phases were designed. The green body of the β-SiAlON-matrix ceramic samples were obtained by using stereolithography (SLA) additive manufacturing. After degreasing, dense β-SiAlON ceramics with different SiAlON phases were fabricated through gas pressure sintering at 1800 °C for 1 hour at GPa. The effects of the different Al_2O_3 contents on the shrinkage, phase composition, relative density, microstructure, mechanical property and hardness were studied. The results indicate that the main phase of the ceramics was β-SiAlON and the specific chemical compositions of it were Si_5AlON_7, $Si_{3.1}Al_{2.9}O_{2.9}N_{5.1}$ and $Si_2Al_4O_4N_4$. The intergranular phases that exists were mainly $Y_3Al_5O_{12}$, $YAlO_3$ and Al_2O_3. With a relative density of 90.03 %, the Vickers hardness (Hv5), bending strength and fracture toughness of the fabricated β-Si_5AlON_7 ceramics were 16.8 GPa, 465 MPa and 4.84 MPa·$m^{1/2}$, respectively. Meanwhile, the shrinkage of the materials was 28.7 %

INTRODUCTION

SiAlON ceramic is a material that was discovered by Oyama [1] and Jack [2] in the study of Si_3N_4 additives in the 1970s. Its crystal structure is the same as silicon nitride, for it also contains α-SiAlON and β-SiAlON crystal structures [3]. β-SiAlON is in accordance with the common formula of $Si_{6-z}Al_zO_zN_{8-z}$, in which Z takes the value from 0 to 4.2 [4, 5]. The performance of β-SiAlON is closely related to the Z value. The results show that the density, hardness, modulus of elasticity, flexural strength and thermal expansion coefficient of β-SiAlON decreased with an increase in the Z value [6]. It has been reported that, compared to α-SiAlON, β-SiAlON exhibits enhanced fracture toughness and strength as well as high thermal conductivities and thermal shock resistance due to the rod-shaped grain structure [7, 8]. Because of its outstanding mechanical and thermal properties at high temperatures, and its excellent chemical stability and thermal shock resistance, β-SiAlON has been attracting considerable attention as an important high-temperature resistant ceramic [9-12].

At present, the forming methods of SiAlON ceramics are mainly hot pressing, cold isostatic, gel casting and freeze-drying. However, it is difficult to obtain a ceramic component with complex shapes by the above forming methods [13-15]. For hot pressing and cold isostatic, it is not economical and convenient to form complex shapes due to the limitations of the mould. When gel casting and freeze-drying are used, the gel and drying processes take dozens of hours or days. Moreover, the fast-drying rate tends to crack the green body, so the drying process has high requirements in the process control. This limits the successful fabrication rate of the green body with complex shapes during the drying process. Because of the inherent hardness and brittleness, it is difficult to achieve the efficient and rapid processing of complex ceramic parts by conventional CNC machining [16]. Therefore, it is of great significance to research a new moulding technology for manufacturing the ceramic with complex shapes.

In recent years, by using digital forming technology, additive manufacturing (AM) has been widely used to fabricate precise parts with complex structures, and it is also a feasible method for fabricating ceramics [17]. This new approach is more efficient than conventional shaping methods in fabricating ceramic parts with complex geometries. Stereolithography (SLA) is an additive manufacturing process that works by focusing an ultraviolet (UV) laser on the photosensitive resin [18]. With the help of CAM or CAD software, a UV laser is used to draw a pre-programmed design or shape on the surface of the photopolymer resin [19]. The photosensitive resin is sensitive to ultraviolet light, so the resin can photochemically solidify and form a single layer of the desired 3D object [20]. This process can be repeated in each layer

of the design until the 3D object is completed. With this method, a variety of ceramics [21-23] and the ceramic precursor [24-26] green bodies have been successfully printed. However, among the printing of the ceramic bodies, most of them were focused on oxide ceramics, a few were reported on nitride ceramics [27]. Therefore, it is extremely essential to develop 3D printing and performance research for nitride-matrix ceramic materials.

In this paper, nitride-matrix ceramic bodies were prepared by the SLA technique, and β-SiAlON ceramics were fabricated via gas pressure sintering. X-ray diffraction (XRD) and field emission scanning electron microscopy (FE-SEM) have been used to study the phase and microstructure of the β-SiAlON ceramics. The purposes of this study are to employ a stereolithography-based additive manufacturing process to fabricate SiAiON ceramics with complex shapes, to demonstrate the difference between the porosity and mechanical property of the β-SiAlON ceramics at the different Z values and to evaluate the effects of the microstructure on the SiAiON ceramics' mechanical properties.

Table 1. The raw materials.

Z value	Si_3N_4	AlN	Al_2O_3	Y_2O_3	Total
			(wt. %)		
$Z = 2$	63.3	10.5	21.4	–	–
$Z = 3$	47.3	14.9	33.0	4.8	100
$Z = 4$	31.3	18.3	45.6	–	–

Table 2. The compositions of the slurry.

Materials	Function	Weight percent (%)
α-Si_3N_4	Raw powder	65
Al_2O_3	Raw powder	–
AlN	Raw powder	–
Y_2O_3	Sintering aids	–
PPTTA	Resin	12.5
PUA	Resin	7
HDDA	Resin	10.5
Capryl alcohol	Resin	5
(PEG-300)	Photoinitiator	1

EXPERIMENTAL

Powder mixture preparation

β-SiAlON ceramics with different theoretical *Z* values were designed by adjusting the ratio of Al_2O_3 and AlN to Si_3N_4 in the raw material. In order to facilitate the writing and reading, this paper mainly discusses and analyses the changes in the *Z* value. In addition, if there is no special explanation in the text, the Z value mainly refers to the theoretical design value.

α-Si_3N_4, AlN and Al_2O_3 powders were used as the starting materials. Yttrium oxide (Y_2O_3) was used as the sintering aid. The total concentration of the sintering aid was 5 wt. % based on the starting materials. The composition design of the raw powders and resin-based ceramic slurry are listed in Table 1 and Table 2, respectively.

The pre-mixed solution of the ceramic slurry consisted of five parts: Ethoxylated (5) pentaerythritol tetraacrylate (PPTTA), Polyurethane acrylate (PUA), Hexanediol Diacrylate (HDDA), Capryl alcohol and Polyethylene glycol (PEG-300). In this paper, using PEG-300 as the photoinitiator, the mass fraction of the photoinitiator was selected to be 1 wt. % of the premixed solution. The characteristics of the various starting materials are listed in Table 3.

Preparation of the ceramic slurry

The light curing resin and the dispersant were prepared in a beaker of the premixed solution. Then the ceramic powder was added into the premixed solution in proportion and the ceramic slurry was ball-milled for 12 h using a zirconia ball. The slurry was then degassed for 0.5 h using a vacuum mixer. Then, the photoinitiator was added into the slurry and mixed for 2 h.

Preparation and post processing of the SiAlON green body

The preparation of the SiAlON ceramics was divided into the following steps: The first step, the ceramic slurry was cast onto a glass slab. The second step, the ceramic

Table 3. The characteristics of the major starting materials.

Materials	Manufacturer	Characteristics
α-Si_3N_4	Yinuo Nitride Co. Ltd. China	99.0 %, 3-5 μm
Al_2O_3	Fuguang Co. Ltd. China 99	99.5 %, 1-5 μm
AlN	Yinuo Nitride Co. Ltd. China	99.5 %, 3-5 μm
Y_2O_3	Yinuo Nitride Co. Ltd. China	99.9 %, 1-3 μm
PPTTA	Curease Chemical Co. Ltd. China	99.9 %, liquid
PUA	Curease Chemical Co. Ltd. China	99.9 %, liquid
HDDA	Curease Chemical Co. Ltd. China	99.9 %, liquid
Capryl alcohol	Aladdin Reagents Co. Ltd. China	99.9 %, liquid
(PEG-300)	Aladdin Reagents Co. Ltd. China	99.5 %, liquid

slurry was subjected to photo-curing using a UV light source, the average power of the UV light source was 60 $mW \cdot cm^{-2}$ and the exposure time was 30 s in order to obtain a single layer of the silicon nitride green body. After the first layer cured, the supporting platform was then moved up, and the ceramic suspension was recoated by a blade on the cured surface. Then, this step repeated until a sufficient thickness of the ceramic green body was obtained. In the third step, the vacuum debinding of the green body was carried out in a vacuum oven at 700 °C for 1 h. Afterwards the residual substances were burnt out at 650 °C for 2 h in air with a 1 $°C \cdot min^{-1}$ heating rate. During the vacuum degreasing process, the cured photosensitive resin was cleaved and small molecular gases escaped. After the cracking, the residual cracked carbon presented between the particles. The oxidation treatment was carried out in the air to completely oxidize the residual carbon in order for it to escape as a gas. The gas pressure sintering of the ceramics was carried out in a Si_3N_4 powder bed at 1800 °C for 1 h in an N_2 atmosphere under 3 MPa.

Mechanical performance testing and microstructure analysis

The flexural strength was tested via the three-point bending method using rectangular bars (3 × 4 × 34 mm) in a universal testing machine (Istron-5569, Instron Group, USA) with a span of 30 mm. The fracture toughness measurement was performed using single-edge-notch beam (SENB) method. The phase analysis was undertaken by X-ray diffraction (XRD; Rigaku D/Max 2200VPC, Japan). The quantitative analysis was determined by comparing the peak intensity of the ratios. The microstructure was examined by scanning electron microscopy (SEM; SUPRA™ 55, ZEISS Co., German). The density was calculated according to the Archimedes principle and the hardness was tested by a Digital Vickers hardness tester (HV5; HVS-30, Shangcai Testermachine Co., Ltd. China) and the porosity of the samples was calculated by the following formula:

$$P = (1 - \rho_o/\rho) \times 100\% \quad (1)$$

where P – the porosity of the porous ceramic, ρ_o – the density of the porous ceramic, ρ – the theoretical density of the dense ceramic.

RESULTS AND DISCUSSION

Dimensional changes during the ceramic preparation

The dimensional change of the material can be divided into two stages: the resin pyrolysis and sintering densification. The first stage was mainly caused by the cracking of the photosensitive resin in the green body and the residual carbon oxidation. In this stage, the decomposition and oxidation of the organic matter with an interparticle bonding were mainly involved. Since there was no external force during the freeze-drying and cold pressing process, the process of the physical densification did not occur between the particles, which caused a little change in the sample size. The second stage was the shrinkage volume caused by the densification of the solid particles. As the traditional sintering densification process, the size of the sample changed significantly during this stage. It can be seen from Table 4 that the dimensional shrinkage rate of the material after sintering was between 28.7 % and 31.6 %. When Z = 4, the shrinkage rate of the material was the highest, however, on the contrary, the porosity rate of the material was the lowest.

Phase analysis

The effects of the different Z values on the phase evolution of the products are shown in Figure 1. After sintering, the main crystalline phases were Si_5AlON_7, $Si_{3.1}Al_{2.9}O_{2.9}N_{5.1}$ and $Si_2Al_4O_4N_4$. These three phases all belong to β-SiAlON. The diffraction peak of $Y_3Al_5O_{14}$, Al_2O_3 (Z = 2) and $YAlO_3$ (Z = 3) were also found. However, no diffraction peaks of Si_3N_4 and AlN were observed in the sintered samples, which meant that all the powders of Si_3N_4 and AlN had completely reacted with Al_2O_3. The formation reactions of the generated phase, as β-SiAlON, $Y_3Al_5O_{14}$ and $YAlO_3$, can be explained by the following equations:

$$Si_3N_4 + Al_2O_3 + AlN \rightarrow Si_{6-Z}Al_ZO_ZN_{8-Z} \quad (2)$$

$$Y_2O_3 + Al_2O_3 \rightarrow Y_3Al_5O_{12} \quad (3)$$

$$Y_2O_3 + Al_2O_3 \rightarrow YAlO_3 \quad (4)$$

With an increase in the amount of Al_2O_3 in the raw materials, the diffraction peak of the SiAlON apparently moved to the left. According to Bragg's law, a decrease

Table 4. The dimensional changes during the ceramic sample preparation (radial direction).

Z value	Green body (mm)	After degreasing (mm)	Sintered (mm)	Shrinkage (%)	Density (cm^3)	Porosity (Block) (%)
Z = 2	50	48.3	35.7	28.7	3.15	9.97
Z = 3	50	48.5	34.9	30.2	3.07	9.20
Z = 4	50	48.1	34.2	31.6	3.04	8.21

in the θ means an increase in the *d* (incident wavelength constant). This indicates that there were more [Al^{3+}] and [O^{2-}] replacing the [Si^{4+}] and [N^{3-}] in the Si_3N_4. The analysis of the product shows that with an increase in the amount of Al_2O_3, the Z value of the generated phase increased from 1 to 4. Meanwhile, in this experiment, the Z value of the reaction product did not match with the theoretical calculation. In other words, when the theoretical designed value of $Z \leq 3$, the Z value of the generated SiAlON phase was lower than the theoretical one. However, when the theoretical value of $Z = 4$, the generated SiAlON phase was consistent with the theoretical calculation. The difference was attributed to the chemical constitution of the intergranular phase. When $Z = 2$, the as-sintered samples, except for the Si_5AlON_7 phase, phases of $Y_3Al_5O_{14}$ and Al_2O_3 also existed. It shows that the phases were formed by the crystallisation of Al_2O_3 and the high aluminate ($Y_3Al_5O_{14}$) at the grain boundary, and this process consumed some of the [Al^{3+}] that should be incorporated into the Si_3N_4 crystal structure.

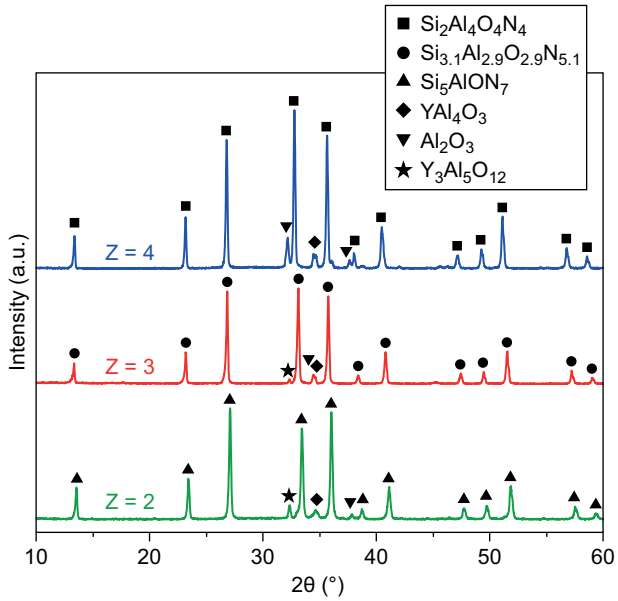

Figure 1. The XRD patterns obtained for the polished surfaces of the β-SiAlON matrix ceramic body after sintering.

With an increase in the amount of Al_2O_3 and AlN ($Z = 4$), only $YAlO_3$, except for $Si_2Al_4O_4N_4$, existed after sintering, and, in this process, the Al_2O_3 consumption of the grain boundary phase was less than that of $Z = 2$. In addition, when under high temperature, the relative content of the liquid phase increased (compared with $Z = 2$), which promoted the replacement process of the [Al^{3+}] and [O^{2-}] with the [Si^{4+}] and [N^{3-}] and this was beneficial for the formation of the high Z value ceramics. Meanwhile, considering the chemical reaction between the Al_2O_3 and Y_2O_3, the Al_2O_3 in the raw material was excessive, so there would be more [Al^{3+}] and [O^{2-}] to replace the [Si^{4+}] and [N^{3-}], which made the *Z* value of the product close to or the same as the theoretical calculation. Therefore, in order to obtain a high *Z* value β-SiAlON ceramic, the content of the aluminium in the raw composition powders should be increased in the design stage.

Microstructure

Figure 2 shows the microstructure of the sintered body observed in the secondary electron (SE) mode. As the *Z* value increased, the grain size also increased.

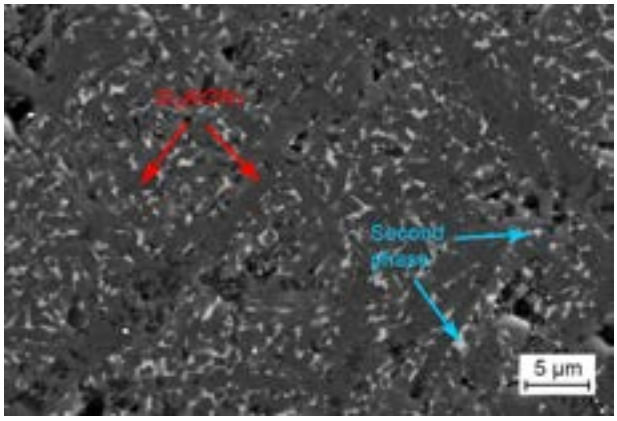

a) $Z = 2$

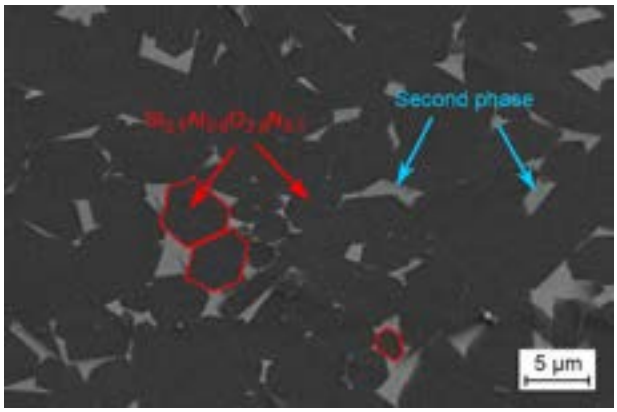

b) $Z = 3$

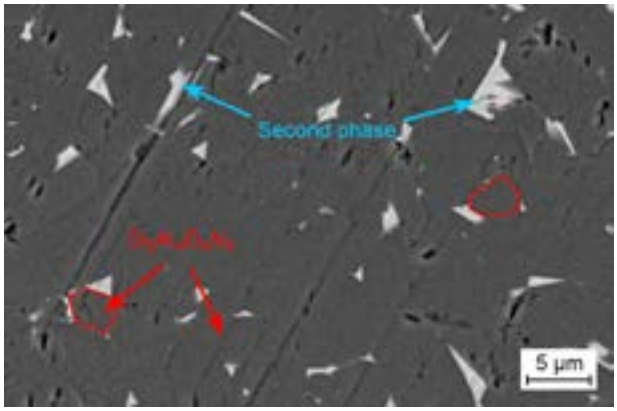

c) $Z = 4$

Figure 2. The SEM micrographs of β-SiAlON: a) $Z = 2$, b) $Z = 3$, c) $Z = 4$.

It is well known that the formation of β-SiAlON ceramics is a dissolution-precipitation process. When the matrix has a higher content of the liquid phase, the dissolution of the silicon nitride in the raw material will be accelerated, and the formation and the growth of the β-SiAlON phase will be promoted. Some studies have also indicated that oxynitride glass network modifiers promote the growth of the β-SiAlON grains with a high aspect ratio [28, 29]. Therefore, a material with a higher *Z* value has a larger grain size, a more complete crystal growth and a grain shape closer to a long rod. In contrast, with a lower *Z* value, some grains are not completely developed, and the aspect ratio of the grain is lower and tends to be equiaxed grains.

Meanwhile, the volume fraction of the intergranular phase increased as the amount of the Al_2O_3 increased. Due to fact that the generation of an excessive intergranular phase weakens the high-temperature mechanical properties and strength, a small amount of the phase was preferable to stay at a level that enabled the densification [30]. Many of the secondary crystalline phases that formed in the sintered silicon-based ceramics' liquid phase were not stable at high temperatures, and the post-densification heat treatment was propitious to reduce the volume fraction of the residual glass. Of course, obtaining a complete crystal is very difficult even if the chemistry of the starting powder mixture is carefully designed [31].

Effects of the *Z* value on the mechanical properties

The bending strength at room temperature of these samples lay in the range of 393-465 MPa (Figure 3). The typical fractured surface after the bending test is shown in Figure 4. When the *Z* value increased from 2 to 4, the bending strength of the β-SiAlON decreased from 465 MPa to 393 MPa. The mechanical properties such as the bending strength of the materials with different porosities and crystal phases were mainly affected by the porosity (or density) and the relative content of the main crystalline phase. The pores in the matrix materials reduced the bearing area and the stress was concentrated in the region near the pores. The strength and the hardness of the material with lower pores was higher. When the porosity was close to each other, the bending strength of the material was mainly affected by the phase structure of the main crystal phase. A higher *Z* value implied that more [Al^{3+}] and [O^{2-}] ions were solid-solved into the silicon nitride crystal, resulting in an increase in the cell size while weakening the robustness. Therefore, the bending strength of the β-SiAlON decreased with an increase in the *Z* value.

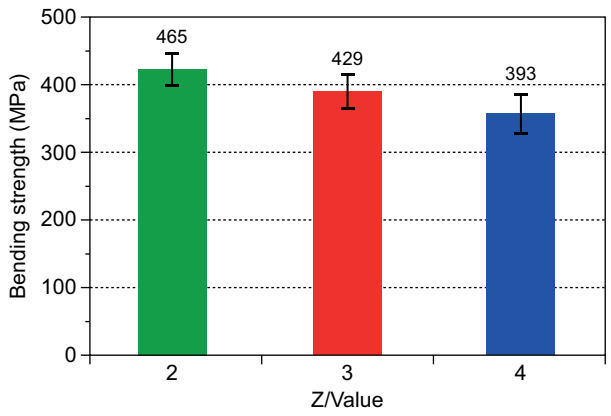

Figure 3. The bending strength variations with the different *Z* values.

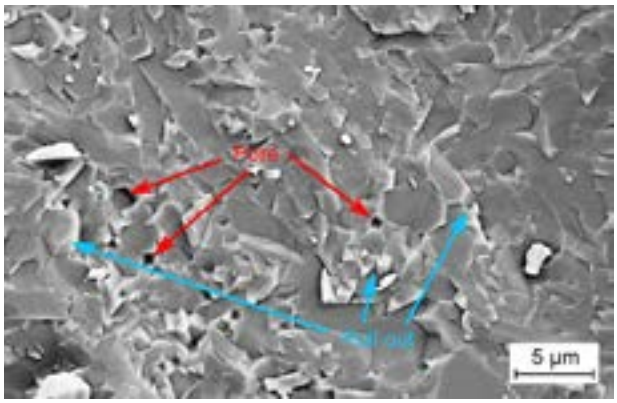

a) *Z* = 2

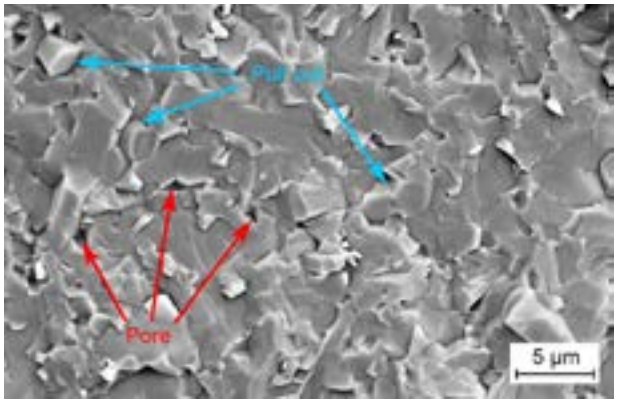

b) *Z* = 3

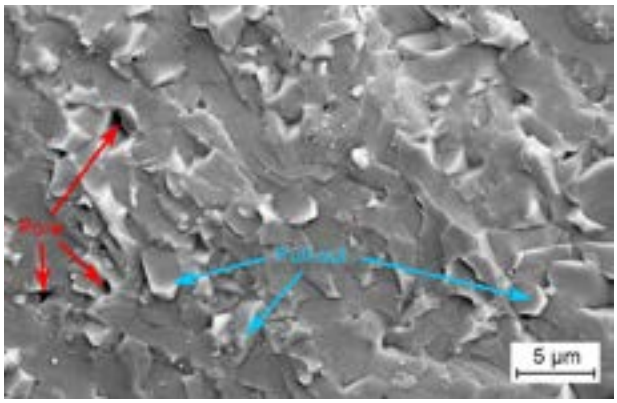

c) *Z* = 4

Figure 4. The SEM pictures of the ceramic materials fracture surface: a) *Z* = 2, b) *Z* = 3, c) *Z* = 4.

From Figure 4, it can be seen the fracture mode was a composite fracture, namely an intergranular fracture and a transgranular fracture exist at the same time. With an increase in the *Z* value, the ratio of the intergranular fractures increased, but the main fracture mode was still a transgranular fracture. Moreover, the pullout phenomenon of the rod-like grains was not obvious. This was mainly due to the high bonding strength between the SiAlON phase and the intergranular phase, which made it difficult for the crack to deflect at the interface joint. However, the existence of the transgranular fracture mode was not conducive to the improvement of the fracture toughness of the materials. Studies have shown that the self-breaking of the rod-like grains controls the high strength. The existence of the intergranular phase indicates the presence of a weak grain boundary structure that was suitable for the crack deflection and pullout during the fracturing. In fact, without the whisker microstructure, a high toughness and high strength would be very difficult to achieve in the SiAlON-based ceramic materials [32]. In general, the densification of β-SiAlON can be accelerated by more liquid phases and a lower viscosity [33-37]. A higher *Z* value (if you add more Al_2O_3 and AlN) would induce more liquid phases during the sintering. Therefore, the apparent porosity (AP) of the β-SiAlON with a higher *Z* value is lower than those with a lower *Z* value. The AP change of the sample can be determined by the SEM micrographs of the fracture surface of the β-SiAlON sample (Figure 4).

The fracture toughness and Vickers hardness with the different *Z* values are given in Figure 5 and 6, respectively. The standard deviation of the fracture toughness and the hardness were changing between ± 0.44 and ± 1.53. When $Z = 4$, the standard deviation was at a maximum for the SiAlON ceramics due to the homogeneities in the microstructure. Both the fracture toughness and the hardness decreased with an increase in the *Z* value. However, the changes were not significant. The fracture toughness of the SiAlON composites can be controlled by the microstructure and it is mainly affected by the grain morphology, the bonding strength between the grain and grain boundary phase, the nature of the crystalline and the different *Z* values.

From Figure 5, it shows that the fracture toughness was between 4.42 and 4.84 MPa·m$^{1/2}$. All of the samples exhibited relatively high fracture toughness values, which were higher than that of the typical equiaxed-grain β-SiAlON (~3.0 MPa·m$^{1/2}$). As shown in Figure 4a, because all samples have elongated and high aspect ratio particles, these elongated grains could toughen the mechanisms, such as the crack deflection, the crack bridging and the grain pullout [38, 39]. A rough fracture face (compared with $Z = 4$) and massive smooth facet holes were observed when $Z = 2$ (Figure 4a), which implied that glassy phase could be readier to cause a crack deflection along either the equiaxed or elongated grains during the crack propagation by weakening the bonding force between the SiAlON and the intergranular phase particles. All the samples at the grain boundary had inter-granular phase particles, and these intergranular phases had a similar bonding strength between the grain and the grain boundary phases. Hence, they had a similar fracture toughness.

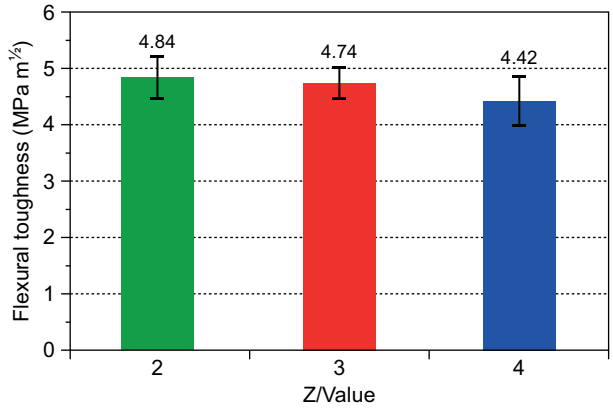

Figure 5. The fracture toughness variations with the change in the *Z* values.

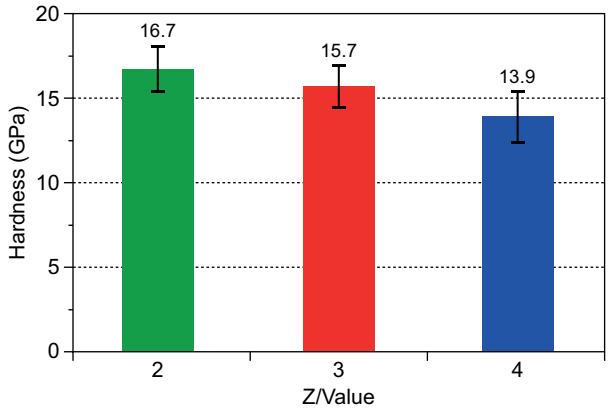

Figure 6. The Vickers hardness variations with the different *Z* values.

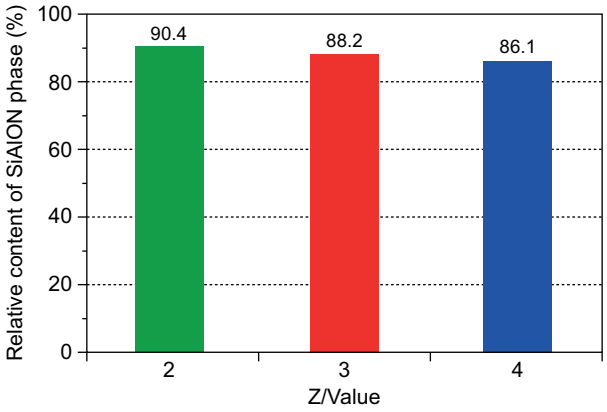

Figure 7. The relative content of the β-SiAON phase in the matrix with the different *Z* values.

Because of the incomplete densification of the matrix materials, holes presented between the SiAlON particles and the intergranular phase particles. The crack tip deflected during the expansion process, and the fracture toughness of the material was improved while consuming part of the fracture energy. Besides, the thermal expansion coefficient was mismatched between the SiAlON matrix (3×10^{-6} K^{-1}) and the intergranular phase as $Y_3Al_5O_{12}$ (7.8×10^{-6} K^{-1}), $YAlO_3$ (2.0×10^{-6} K^{-1}/a axis, 8.7×10^{-6} K^{-1}/c axis) leading to micro-cracking which is also a major mechanism for the improvement in the toughness of the composites.

The hardness of the SiAlON ceramics was controlled by the relative content of the main phase. However, the microstructure of the porosity, grain size, shape and orientations, intergranular phase and the *Z* value, etc., also affected the hardness, but less prominently than the content of the main phase. The hardness of the β-SiAlON ceramics varied between 16.7 GPa and 13.9 GPa, for the samples had a similar β-SiAlON amount (86.1 - 90.4 %, Figure 7), a similar grain boundary phase nature (crystalline) and a porosity level for the different *Z* values (8.21 - 9.97 %, Table 3). As mentioned above, due to the fact that the Z value increased, more [Al^{3+}] and [O^{2-}] ions were solid-solved into the silicon nitride crystal resulting in an increase in the cell size while weakening the robustness. Therefore, the sample with $Z = 2$ had the highest hardness compared to the other two sets of samples. Figure 8 shows the β-SiAlON ceramics fabricated by the stereolithography-based additive manufacturing (after polishing).

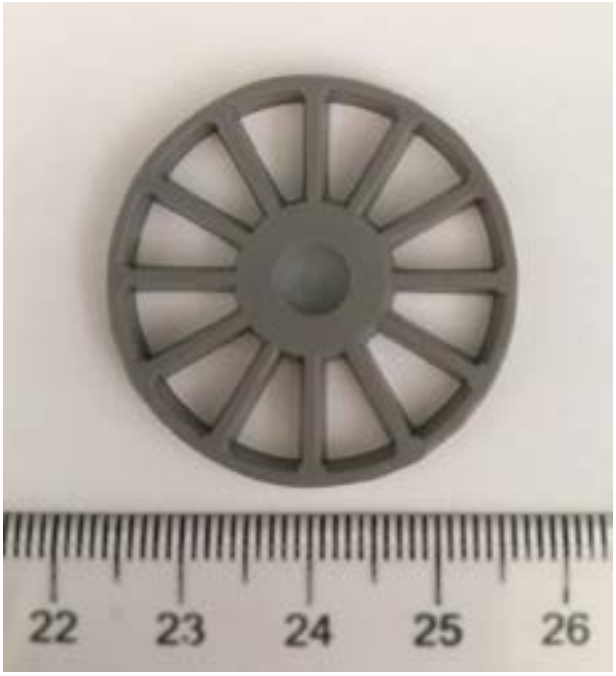

Figure 8. The β-SiAON ceramic manufactured by the stereolithography-based additive manufacturing.

CONCLUSIONS

In this paper, using Si_3N_4, Al_2O_3 and AlN as the raw materials, β-SiAlON materials with different Z values ($Z = 2, 3, 4$) were successfully fabricated by the additive manufacturing and gas pressure sintering method (1800 °C/1 h/3 GPa). The effects of the *Z* value on the density, crystallisation, microstructure and mechanical properties of the β-SiAlON matrix ceramics have been studied. According to the XRD patterns, with an increase in the *Z* value, the main phases of the β-SiAlON were Si_5AlON_7, $Si_{3.1}Al_{2.9}O_{2.9}N_{5.1}$ and $Si_2Al_4O_4N_4$, respectively. The intergranular phases were mainly $Y_3Al_5O_{12}$, $YAlO_3$ and Al_2O_3. For the β-SiAlON, the density increased with an increase in the *Z* value, while the apparent porosity, bending strength, fracture toughness and hardness decreased accordingly. The bending strength, fracture toughness and Vickers hardness of the β-SiAlON ($Z = 2$) achieved 465 MPa, 4.84 MPa $m^{1/2}$ and 16.7 GPa, respectively. The fracture of the material was a composite fracture mode, but dominated by transgranular fractures.

Acknowledgements

This work was financially supported by Local Innovative and Research Team Project of Guangdong Pearl River Talents Program (Grant No.2017BT01C169), Science and Technology Major Project of Guangdong Province (Grant No. 2016B090915002), Science and Technology Major Project of Guangdong Province (Grant No. 2017B090911011), the China Postdoctoral Science Foundation (CPSF, Grant No. 2018M633013).

REFERENCES

1. Oyama Y., Kamigaito O. (1971): Solid solubility of some oxidesin Si_3N_4. *Japanese Journal of Applied Physics*, *10*(11), 1637. doi: 10.1143/JJAP.10.1637
2. Jack K. H., Wilson W. I. (1972): Ceramics based on the Si–Al–ON and related systems. *Nature Physical Science*, *238*(80), 28. doi: 10.1038/physci238028a0
3. Cao G. Z., Metselaar R. (1991): α-Sialon ceramics: a review. *Chemistry of Materials*, *3*(2), 242-252. doi: 10.1021/cm00014a009
4. Jack K. H. (1976): Sialons and related nitrogen ceramics. *Journal of materials science*, *11*(6), 1135-1158. doi: 10.1007/bf00553123
5. Ekström T., Nygren M. (1992): SiAION ceramics. *Journal of the American Ceramic Society*, *75*(2), 259-276. doi: 10.1111/j.1151-2916.1992.tb08175.x
6. Ekström T., Käll P. O., Nygren M., Olsson P. O. (1989): Dense single-phase β-sialon ceramics by glass-encapsulated hot isostatic pressing. *Journal of Materials Science*, *24*(5), 1853-1861. doi: 10.1007/BF01105715

7. Kushan S. R., Uzun I., Dogan B., Mandal H. (2007): Experimental and Finite Element Study of the Thermal Conductivity of α-SiAlON Ceramics. *Journal of the American Ceramic Society*, *90*(12), 3902-3907. doi: 10.1111/j.1551-2916.2007.01993.x
8. Yi X., Zhang W., Akiyama T. (2014): Thermal conductivity of β-SiAlONs prepared by a combination of combustion synthesis and spark plasma sintering. *Thermochimica Acta*, *576*, 56-59. doi: 10.1016/j.tca.2013.12.002
9. Sabagh S., Bahramian A. R., Kokabi M. (2012): SiAlON nanoparticles effect on the corrosion and chemical resistance of epoxy coating. *Iranian Polymer Journal*, *21*(12), 837-844. doi: 10.1007/s13726-012-0095-1
10. Ryu J. H., Park Y. G., Won H. S., Kim S. H., Suzuki H., Yoon C. (2009). Luminescence properties of Eu^{2+}-doped [beta]-$Si_{6-z}Al_zO_zN_{8-z}$ microcrystals fabricated by gas pressured reaction. *of Crystal Growth*, *311*(3), 878-882. doi: 10.1016/j.jcrysgro.2008.09.107
11. Ryu J. H., Park Y. G., Won H. S., Kim S. H., Suzuki H., Yoon C. (2009): Synthesis and photoluminescence properties of beta-sialon: Eu^{2+} ($Si_{6-z}Al_zO_zN_{8-z}$: Eu^{2+}). *Journal of Crystal Growth*, *311*(3), 878-882. doi: 10.1149/1.2768289
12. Xu X., Nishimura T., Hirosaki N., Xie R. J., Yamamoto Y., Tanaka H. (2005): Fabrication of β-sialon nanoceramics by high-energy mechanical milling and spark plasma sintering. *Nanotechnology*, *16*(9), 1569. doi: 10.1088/0957-4484/16/9/027
13. Ye F., Hou Z., Zhang H., Liu L., Zhou Y. (2010): Spark plasma sintering of cBN/β-SiAlON composites. *Materials Science and Engineering: A*, *527*(18-19), 4723-4726. doi: 10.1016/j.msea.2010.04.034
14. Liu G., Attallah M. M., Loretto M., Herny E., Jiang Y., Button T. W. (2015): Gel casting of sialon ceramics based on water soluble epoxy resin. *Ceramics International*, *41*(9), 11534-11538. doi: 10.1016/j.ceramint.2015.05.081
15. Hou Z., Ye F., Liu L., Liu Q. (2012): Fabrication of gradient porous β-SiAlON ceramics via a camphene-based freeze casting process. *Materials Science and Engineering: A*, *558*, 742-746. doi: 10.1016/j.msea.2012.08.094
16. Li Y., Ge B., Wu Z., Xiao G., Shi Z., Jin Z. (2017): Effects of h-BN on mechanical properties of reaction bonded β-SiAlON/h-BN composites. *Journal of Alloys and Compounds*, *703*, 180-187. doi: 10.1016/j.jallcom.2017.01.318
17. Bártolo P. J. (Ed.). (2011). Stereolithography: materials, processes and applications. Springer Science & Business Media.pp. 41-43.
18. Crivello J. V., Reichmanis E. (2013): Photopolymer materials and processes for advanced technologies. *Chemistry of Materials*, *26*(1), 533-548. doi: 10.1021/cm402262g
19. Lipson H., Moon F. C., Hai J., Paventi C. (2004). 3-D printing the history of mechanisms. *Journal of Mechanical Design*, *127*(5), 1029-1033. doi:10.1115/1.1902999
20. Fouassier J. P., Lalevée J. (2012). Photopolymerization Reactions, Chapter 4, in: *Photoinitiators for polymer synthesis: scope, reactivity, and efficiency*. John Wiley & Sons. Pp.41-72. doi: 10.1002/9783527648245.ch4
21. Trombetta R., Inzana J. A., Schwarz E. M., Kates S. L., Awad H. A. (2017): 3D printing of calcium phosphate ceramics for bone tissue engineering and drug delivery. *Annals of Biomedical Engineering*, *45*(1), 23-44. doi: 10.1007/s10439-016-1678-3
22. Song S. Y., Park M. S., Lee J. W., Yun J. S. (2018): Improvement of dispersion stability and 3D-printing characteristics of ceramics in photopolymers by controlling the coating thickness of silane coupling agents. *Materials Chemistry and Physics*, *216*, 446-453. doi: 10.7735/ksmte.2018.27.2.140
23. Wu H., Cheng Y., Liu W., He R., Zhou M., W, S.,Song X., Chen Y. (2016): Effect of the particle size and the debinding process on the density of alumina ceramics fabricated by 3D printing based on stereolithography. *Ceramics International*, *42*(15), 17290-17294. doi: 10.1016/j.ceramint.2016.08.024
24. Li S., Duan W., Zhao T., Han W., Wang L., Dou R., Wang G. (2018): The fabrication of SiBCN ceramic components from preceramic polymers by digital light processing (DLP) 3D printing technology. *Journal of the European Ceramic Society*, *38*(14), 4597-4603. doi: 10.1016/j.jeurceramsoc.2018.06.046
25. Eckel Z. C., Zhou C., Martin J. H., Jacobsen A. J., Carter W. B., Schaedler T. A. (2016): Additive manufacturing of polymer-derived ceramics. *Science*, *351*(6268), 58-62. doi: 10.1126/science.aad2688
26. de Hazan Y., Penner D. (2017): SiC and SiOC ceramic articles produced by stereolithography of acrylate modified polycarbosilane systems. *Journal of the European Ceramic Society*, *37*(16), 5205-5212. doi: 10.1016/j.jeurceramsoc.2017.03.021
27. Tian Z., Yang Y., Wang Y., Wu H., Liu W., Wu S. (2019): Fabrication and properties of a high porosity h-BN-SiO_2 ceramics fabricated by stereolithography-based 3D printing. *Materials Letters*, *236*, 144-147. doi: 10.1016/j.matlet.2018.10.058
28. Björklund H., Wasén J., Falk L. K. (1997): Quantitative Microscopy of β-Si_3N_4 Ceramics. *Journal of the American Ceramic Society*, *80*(12), 3061-3069. doi: 10.1111/j.1151-2916.1997.tb03233.x
29. Björklund H., Falk L. K. L., Rundgren K., Wasén J. (1997): β-Si_3N_4 grain growth, part I: Effect of metal oxide sintering additives. *Journal of the European Ceramic Society*, *17*(11), 1285-1299. doi: 10.1016/S0955-2219(96)00237-3
30. Lange F. F. (1974): High-temperature strength behavior of hot-pressed Si_3N_4: evidence for subcritical crack growth. *Journal of the American Ceramic Society*, *57*(2), 84-87. doi: 10.1111/j.1151-2916.1974.tb10819.x
31. Zhao Z., Johnsson M., Shen Z. (2002): Microstructure and mechanical properties of titanium carbonitride whisker reinforced β-sialon matrix composites. *Materials Research Bulletin*, *37*(6), 1175-1187. doi: 10.1016/S0025-5408(02)00738-9
32. Zeuner M., Pagano S., Schnick W. (2011): Nitridosilicates and oxonitridosilicates: from ceramic materials to structural and functional diversity. *Angewandte Chemie International Edition*, *50*(34), 7754-7775. doi: 10.1002/9783527631940.ch60
33. Çalışkan F., Tatlı Z., Genson A., Hampshire S. (2012): Pressureless sintering of β-SiAlON ceramic compositions using fluorine and oxide additive system. *Journal of the European Ceramic Society*, *32*(7), 1337-1342. doi: 10.1016/j.jeurceramsoc.2011.05.016
34. Eser O., Kurama S., Gunkaya G. (2010): The production of β-SiAlON ceramics with low amounts of additive, at low sintering temperature. *Journal of the European Ceramic Society*, *30*(14), 2985-2990. doi: 10.1016/j.jeurceramsoc.2010.01.024

35. Mallik A. K., Acikbas N. C., Kara F., Mandal H., Basu D. (2012): A comparative study of SiAlON ceramics. *Ceramics International*, *38*(7), 5757-5767.doi: 10.1016/j.ceramint.2012.04.022
36. German R. M., Suri P., Park S. J. (2009): Review: liquid phase sintering. *Journal of Materials Science*, *44*(1), 1-39. doi: 10.1007/s10853-008-3008-0
37. Kingery W.D., Bowen H.K., Uhlmann D.R. (1976). *Introduction to Ceramics*, 2nd ed., Wiley-Interscience, New York.
38. Lee S. G., Kim Y. W., Mitomo M. (2001): Relationship between microstructure and fracture toughness of toughened silicon carbide ceramics. *Journal of the American Ceramic Society*, *84*(6), 1347-1353. doi: 10.1111/j.1151-2916.2001.tb00840.x
39. Yu Z. B., Thompson D. P. (2006). Sialon Part V-18, in: Low I.M. (ed.): *Ceramic-Matrix Composites-Microstructure, Properties and Applications*. Woodhead Publishing. pp 491–513.